

IMMUNOTHERAPY

In vivo CAR T cell generation to treat cancer and autoimmune disease

Theresa L. Hunter¹, Yanjie Bao¹, Yan Zhang¹, Daiki Matsuda¹, Romina Riener¹, Annabel Wang¹, John J. Li¹, Ferran Soldevila¹, David S. H. Chu¹, Duy P. Nguyen¹, Qian-Chen Yong¹, Brittany Ross¹, Michelle Nguyen¹, James Vestal¹, Scott Roberts¹, Diana Galvan¹, Jerel Boyd Vega¹, Donald Jhung¹, Matthew Butcher¹, Josephine Nguyen¹, Stanley Zhang¹, Claudia Fernandez¹, Jeffrey Chen¹, Carolina Herrera¹, Yi Kuo¹, E. Michael Pica¹, Goutam Mondal¹, Andrew L. Mammen², John Scholler³, Steven P. Tanis¹, Stuart A. Sievers¹, Aric M. Frantz¹, Gregor B. Adams¹, Laura Shawver¹, Ramin Farzaneh-Far¹, Michael Rosenzweig¹, Priya P. Karmali¹, Adrian I. Bot¹, Carl H. June^{3,4,5*}, Haig Aghajanian^{1,3*}

Chimeric antigen receptor (CAR) T cell therapies have transformed treatment of B cell malignancies. However, their broader application is limited by complex manufacturing processes and the necessity for lymphodepleting chemotherapy, restricting patient accessibility. We present an in vivo engineering strategy using targeted lipid nanoparticles (tLNPs) for messenger RNA delivery to specific T cell subsets. These tLNPs reprogrammed CD8⁺ T cells in both healthy donor and autoimmune patient samples, and in vivo dosing resulted in tumor control in humanized mice and B cell depletion in cynomolgus monkeys. In cynomolgus monkeys, the reconstituted B cells after depletion were predominantly naive, suggesting an immune system reset. By eliminating the requirements for complex ex vivo manufacturing, this tLNP platform holds the potential to make CAR T cell therapies more accessible and applicable across additional clinical indications.

There are currently six Food and Drug Administration (FDA)-approved CAR T cell therapies on the US market for the treatment of various B cell malignancies, and hundreds more autologous and allogeneic CAR T and CAR natural killer (NK) products are being tested in clinical trials across the world (1). These ex vivo cell therapies have shown remarkable success in providing durable responses to patients with advanced and refractory cancers (2, 3). Unfortunately, access to these therapies has been limited by challenges in manufacturing (costs, time, and scaling), geography, the limited number of specialized CAR T centers, the need for lymphodepleting chemotherapy, and safety concerns about genotoxicity with integrating vectors (4). Recently, CAR T cell therapy has shown great promise in the treatment of patients with B cell-mediated autoimmune disease (5). Emerging case reports indicate that B cell-targeted CAR T cell therapies can provide substantial and lasting clinical benefits in conditions such as systemic lupus erythematosus, myositis, systemic sclerosis, and myasthenia gravis (6–10). These autoimmune diseases affect a considerably larger population than B cell malignancies, with ~20 million individuals in the United States and up to 10% of the

global population impacted by some form of autoimmune disorder—a prevalence that continues to rise (11–13). Addressing such a vast patient population necessitates a therapy that is scalable, off-the-shelf, devoid of cells and integrating viral vectors, does not require chemotherapy, and can be administered outside of specialized centers. An in vivo CAR T approach not requiring lymphodepletion may fulfill these requirements. Accordingly, we developed a novel targeted lipid nanoparticle capable of safely and preferentially engineering human T cells in vivo to become functional CAR T cells and identified a clinically translatable, two-or-three-infusion regimen to safely achieve deep B cell depletion.

Results

Targeted lipid nanoparticle formulations for in vivo T cell engineering

In our prior study of targeted lipid nanoparticle (tLNP) delivery of mRNA payloads for in vivo CAR engineering (14), we used an LNP composition similar to those used in mRNA vaccines. In order for this technology to be used broadly in therapeutics with an acceptable safety profile, we sought to develop a tLNP specifically designed for in vivo mRNA delivery to immune cells. tLNPs consist of a lipid nanoparticle comprising five lipid components—including an ionizable lipid, a targeting moiety conjugated to the LNP (such as an antibody), and an encapsulated mRNA payload (Fig. 1A and table S1). Our tLNP design objectives included reduced functional delivery to the liver, efficient delivery of mRNA to target immune cells, improved biodegradability, reduced reactogenicity, and improved tolerability. We rationally designed ionizable (cationic) lipids and tLNP compositions to impart these characteristics. We formulated one of these novel ionizable lipids, Lipid 829 (L829) into CD5-targeted tLNPs encapsulating an mRNA encoding a luciferase reporter protein. We compared these L829-tLNPs to tLNPs formulated with a benchmark ionizable lipid used in a severe acute respiratory syndrome coronavirus 2 (SARS-CoV-2) vaccine, ALC-0315 (BNT162b2) (15). Bioluminescence imaging revealed that animals treated with benchmark LNP exhibited luciferase expression in the liver and spleen at 6 and 24 hours (Fig. 1B and fig. S1, A and B). By contrast, animals treated with L829-LNP showed significantly lower luciferase expression in both liver and spleen (Fig. 1B and fig. S1, A and B). Administration of anti-CD5 antibody-targeted benchmark tLNP resulted in biodistribution similar to that of the untargeted LNP. However, CD5-L829-tLNP-treated animals showed a specific signal in the spleen without increased off-target liver expression (Fig. 1B and fig. S1, A and B). Reduced off-target delivery to liver and enhanced delivery to T cells compared with benchmark and previous reports (16–18) were also observed when using CD5-L829-tLNPs encapsulating mRNA encoding mCherry protein (fig. S1, C and E). Liquid chromatography-mass spectrometry (LC-MS) analysis showed that L829 lipid was rapidly cleared from the liver in CD5-L829-tLNP-treated mice, whereas ALC-0315 levels remained elevated for at least 7 days, which is consistent with conventional LNP accumulation in the liver (Fig. 1C). To assess whether decreased liver uptake and rapid clearance of L829-LNP translated to an increase in safety and tolerability, we utilized Sprague-Dawley rats and cynomolgus monkeys, which are species sensitive to LNP toxicities (19). Rats treated with human CD5-targeted L829-tLNP had significantly lower levels of acute phase response proteins compared with those treated with the benchmark tLNP (Fig. 1D). Rat CD5-targeted L829-tLNP was well tolerated up to the highest dose of 5 mg/kg, with no adverse observations (fig. S2, A and B). In cynomolgus monkeys, CD5-L829-tLNP was safely administered intravenously up to a high dose of 3 mg/kg, with lower liver enzyme levels when compared with benchmark tLNP-treated animals at the higher doses (Fig. 1E).

Preferential engineering of CD8⁺ T cells

We sought to specifically target the CD8⁺ T cell subset because this approach may be advantageous in certain diseases (20). Selective

¹Capstan Therapeutics, San Diego, CA, USA. ²Muscle Disease Section, National Institute of Arthritis and Musculoskeletal and Skin Diseases, National Institutes of Health, Bethesda, MD, USA. ³Center for Cellular Immunotherapies, Perelman School of Medicine at the University of Pennsylvania, Philadelphia, PA, USA. ⁴Department of Pathology and Laboratory Medicine, Perelman School of Medicine at the University of Pennsylvania, Philadelphia, PA, USA. ⁵Parker Institute for Cancer Immunotherapy at the University of Pennsylvania, Philadelphia, PA, USA. *Corresponding author. Email: haghajanian@capstantx.com (H.A.); cjune@upenn.edu (C.H.J.)

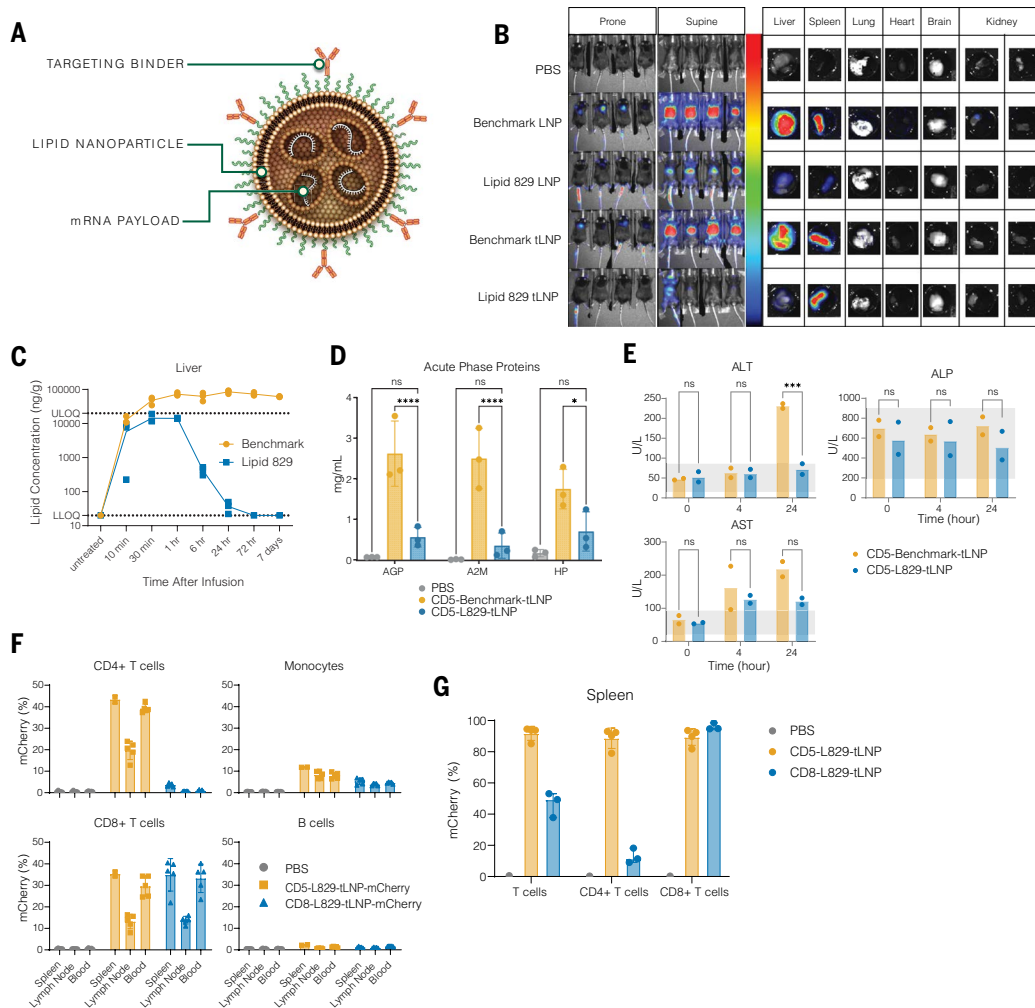


Fig. 1. Ionizable lipid L829 reduces off-target delivery of tLNP to liver. (A) Schematic representation of a targeted lipid nanoparticle. (B) Bioluminescence imaging of WT C57BL/6 mice 6 hours after treatment with CD5 tLNP encapsulating luciferase mRNA. Representative images of five mice per group are shown. Images are scaled at 0 to 250,000 photons/s/mm²/sr. (C) Quantification of benchmark and L829 lipids in WT C57BL/6 mouse liver tissue at indicated time points after treatment with CD5 tLNPs. $n = 3$ mice per time point per group. (D) Plasma levels of acute phase proteins alpha-1 acid glycoprotein (AGP), alpha-2 macroglobulin (A2M), and haptoglobin (HP) in rats 24 hours after dosing with 3.0 mg/kg CD5 tLNP. $n = 3$ rats per group; samples were run in duplicate and averaged. (E) Serum concentration of alanine aminotransferase (ALT), aspartate transferase (AST), and alkaline phosphatase (ALP) in cynomolgus monkeys after a single dose of 3.0 mg/kg CD5 tLNPs. $n = 2$ monkeys per group. Statistical analysis in (D) and (E) performed by two-way analysis of variance (ANOVA) with post hoc multiple comparisons (** $P \leq 0.01$, *** $P \leq 0.001$). Normal reference range is shown by gray shading. (F) Expression of mCherry in CD4⁺ and CD8⁺ T cells, monocytes, and B cells 24 hours after intravenous dosing of 10 μ g tLNP in WT C57BL/6 mice. $n = 5$ mice per group. (G) mCherry expression 24 hours after intravenous dosing of 20 μ g tLNPs in NOD scid gamma (NSG) mice engrafted with human T cells. $n = 3$ to 4 mice per tLNP group. 1 phosphate-buffered saline (PBS) control mouse. Data are mean \pm standard deviation.

expression in CD8⁺ T cells may be important in indications in which CD4⁺ T cell CAR expression and activation could have unwanted effects, such as in autoimmune disease (21). Additionally, CD4⁺ CAR T cells have been shown to be the major driver of cytokine release syndrome (CRS) in patients receiving CAR T therapy (22). To achieve CD8-specific targeting, an antimouse CD8 antibody was conjugated to L829-LNP. Wild-type (WT) mice injected with CD8-L829-tLNP-mCherry preferentially expressed the reporter in CD8⁺ T cells compared with CD4⁺ T cells, B cells, or monocytes (Fig. 1F). Similarly, in humanized mice, CD8-L829-tLNP preferentially engineered human CD8⁺ T cells over CD4⁺ T cells (Fig. 1G). mRNA encoding an antihuman CD19 CAR was also encapsulated in L829-tLNP to produce CAR T cells. In a time-course study, CD8-L829-tLNP rapidly engineered CD8⁺ T cells in the blood, spleen, bone marrow, and lymph nodes of WT mice in a transient manner, with declining expression over 72 hours (fig. S3A). As with

the reporter, selective expression of the CAR was observed on CD8⁺ T cell populations after transfection with CD8-L829-tLNP-CD19 and CAR T cells produced from these tLNP transfections displayed antigen-specific cytotoxicity, proliferation, and cytokine production (fig. S3).

mRNA designed to maximize CAR engineering of human T cells

To enhance the expression and functionality of anti-CD19 CAR T cells, we designed mRNA sequences incorporating various untranslated regions (UTRs) and codon usage strategies. Starting with two second-generation anti-CD19 CAR (23, 24) architectures (Fig. 2A), we designed mRNAs with diverse UTR sequences and codon usage combinations (Fig. 2B). These mRNAs were then encapsulated in L829-tLNPs and incubated with human primary T cells. Cells were evaluated for peak levels and durability of CAR expression (Fig. 2C and fig. S4A). Several constructs demonstrated enhanced CAR expression and increased

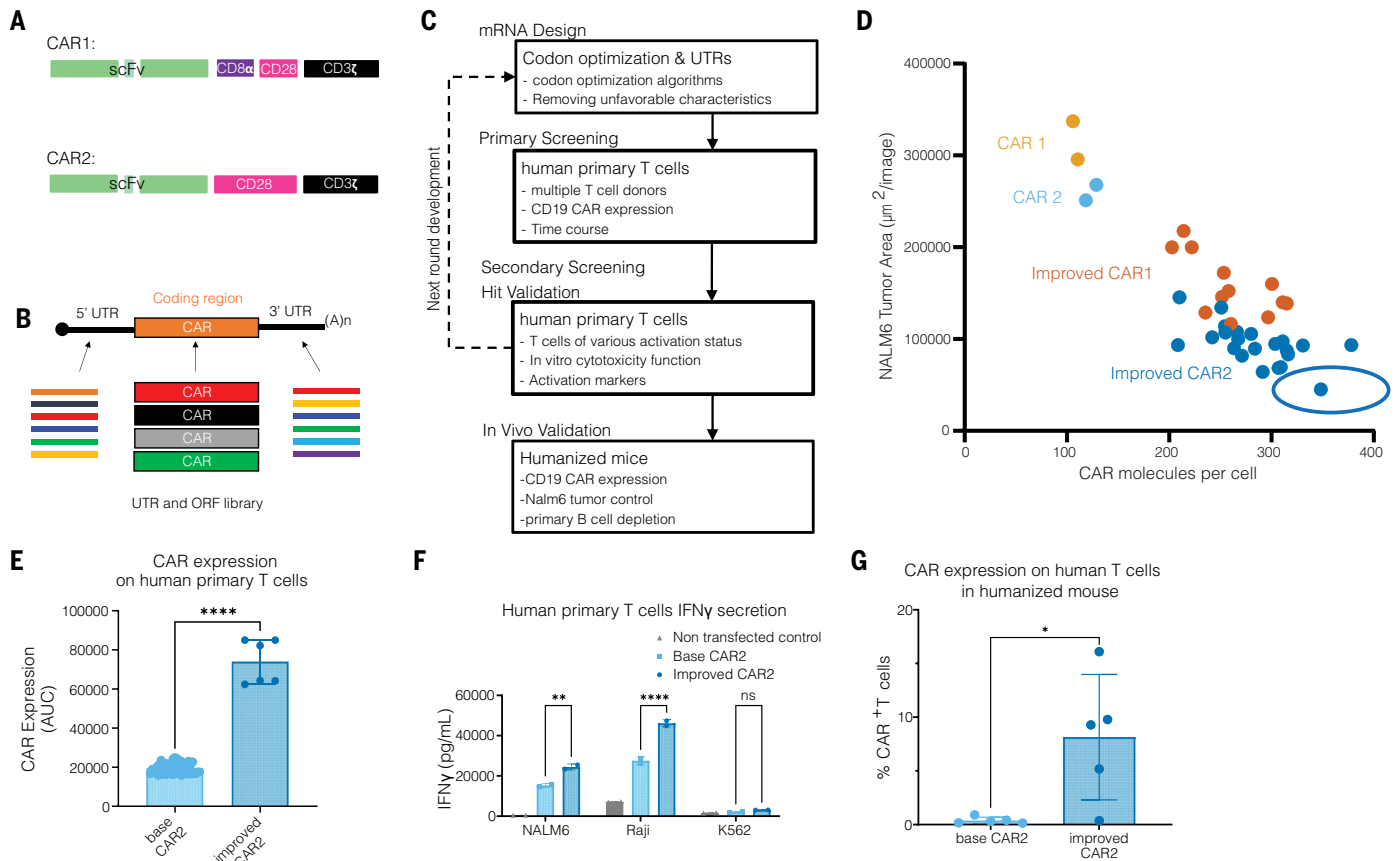


Fig. 2. Enhancements in anti-CD19 CAR mRNA improve expression and function in T cells. (A) Diagrams of tested CAR designs. scFv, single-chain variable fragment. (B) Overview of sequence improvement strategies. ORF, open reading frame. (C) Flowchart of the scheme for selecting and prioritizing mRNA payload development candidates. (D) Freshly activated human T cells were transfected with tLNP encapsulating different CAR mRNA sequences. Anti-CD19 CAR molecules per cell were measured at 48 hours after transfection (x axis) and correlated with Nalm6 tumor cell killing (y axis, Nalm6 tumor area from Incucyte-based killing at 6:1 T cell-to-tumor cell ratio) 48 hours after coculture. Each dot represents a different tested construct; the construct chosen for further analysis is circled in blue. (E) Comparative analysis of CAR expression in expanded human T cells between the original (base) and improved CAR2 construct. CAR expression is represented as area under the curve (AUC) of CAR molecules per cell at 6, 24, and 48 hours after transfection. (F) Expression of IFN γ after coculture with indicated target cells. K562 is a CD19-negative control. (G) CD19 CAR expression in splenic T cells from NCG mice engrafted with human T cells and bearing Nalm6 tumors after three doses with 10 μ g CD5-tLNP with either original or improved mRNA. $n = 5$ mice per group. Statistical analysis in (E) and (G): unpaired two-tailed t test ($*P \leq 0.05$); statistical analysis in (F): two-way ANOVA with post hoc multiple comparisons ($**P \leq 0.01$, $****P \leq 0.0001$). Data are mean \pm standard deviation.

efficiency in lysing of CD19⁺ tumor cells in vitro (Fig. 2D) and performed favorably compared with DNA lentiviral CAR constructs (fig. S4, B and C). An improved CAR2 design was selected for further evaluation; tLNP-generated CAR T cells from this construct demonstrated significantly increased CAR expression, cytokine production, and degranulation in response to CD19⁺ target cells (Fig. 2, E and F, and fig. S4D). This improvement translated in vivo, with significantly higher CAR expression on T cells in humanized mice after intravenous administration (Fig. 2G). Beyond enhanced cytotoxicity, the improved CAR2 sequence enabled expression in nonactivated T cells (fig. S4E), demonstrated dose-dependent cytotoxicity against autologous B cells (fig. S4F), and exhibited serial killing capacity against an antigen-positive tumor cell line (fig. S4G). The cytotoxic function of CD8-L829-tLNP-generated CAR T cells was primarily mediated by CD8⁺ T cells, because depletion of CD4⁺ T cells, NK cells, or monocytes had no apparent effect on B cell lysis across multiple tLNP doses (fig. S4H).

In vivo CAR T efficacy against human primary B cells and tumors

B cell-depleting CAR T cells have shown promising efficacy in treating patients with B cell-mediated autoimmune disease (5). To evaluate the effectiveness of our improved L829-tLNPs in generating functional

CAR T cells from individuals with autoimmune conditions, we obtained PBMCs from patients with autoimmune disease as well as age-matched (+/- 10 years) and sex-matched healthy donors. CD8⁺ T cells from autoimmune patients were phenotypically similar to healthy donor T cells and were comparably engineered into CAR T cells by using CD8-L829-tLNPs (Fig. 3A and fig. S5, A and B). Notably, CAR T cells derived from autoimmune patient samples effectively lysed autologous B cells from these affected individuals (Fig. 3B).

To evaluate in vivo reprogramming of human T cells for targeted B cell elimination, we engrafted human peripheral blood mononuclear cells (PBMCs) into immunocompromised mice. After 17 days of engraftment, mice were intravenously injected with 10 or 30 μ g of CD8-L829-tLNP-CD19. Within 24 hours, B cells were largely eradicated from the spleens in both dosage groups, in contrast to control tLNP-treated mice (Fig. 3C and fig. S5C). CAR expression was predominantly observed in CD8⁺ T cells, with minimal expression in CD4⁺ T cells (fig. S5D). Notably, early assessments indicated B cell depletion as soon as 1 hour after dosing, with near-complete elimination by 3 hours (Fig. 3D and fig. S5E). CAR expression peaked at 6 hours and remained detectable on T cells at 24 hours (Fig. 3E). The duration of B cell depletion was further evaluated with a CD34⁺ hematopoietic stem cell humanized

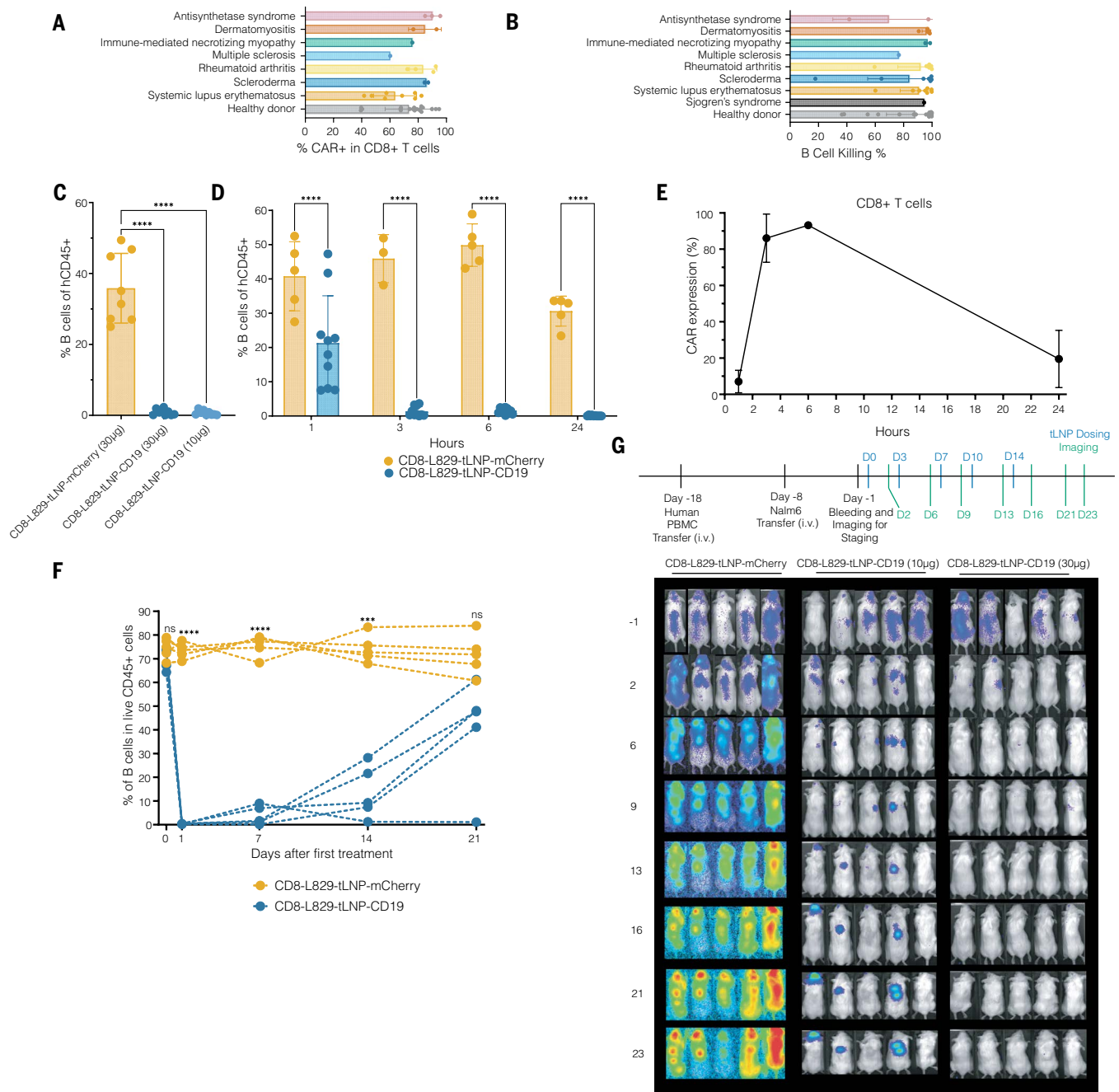
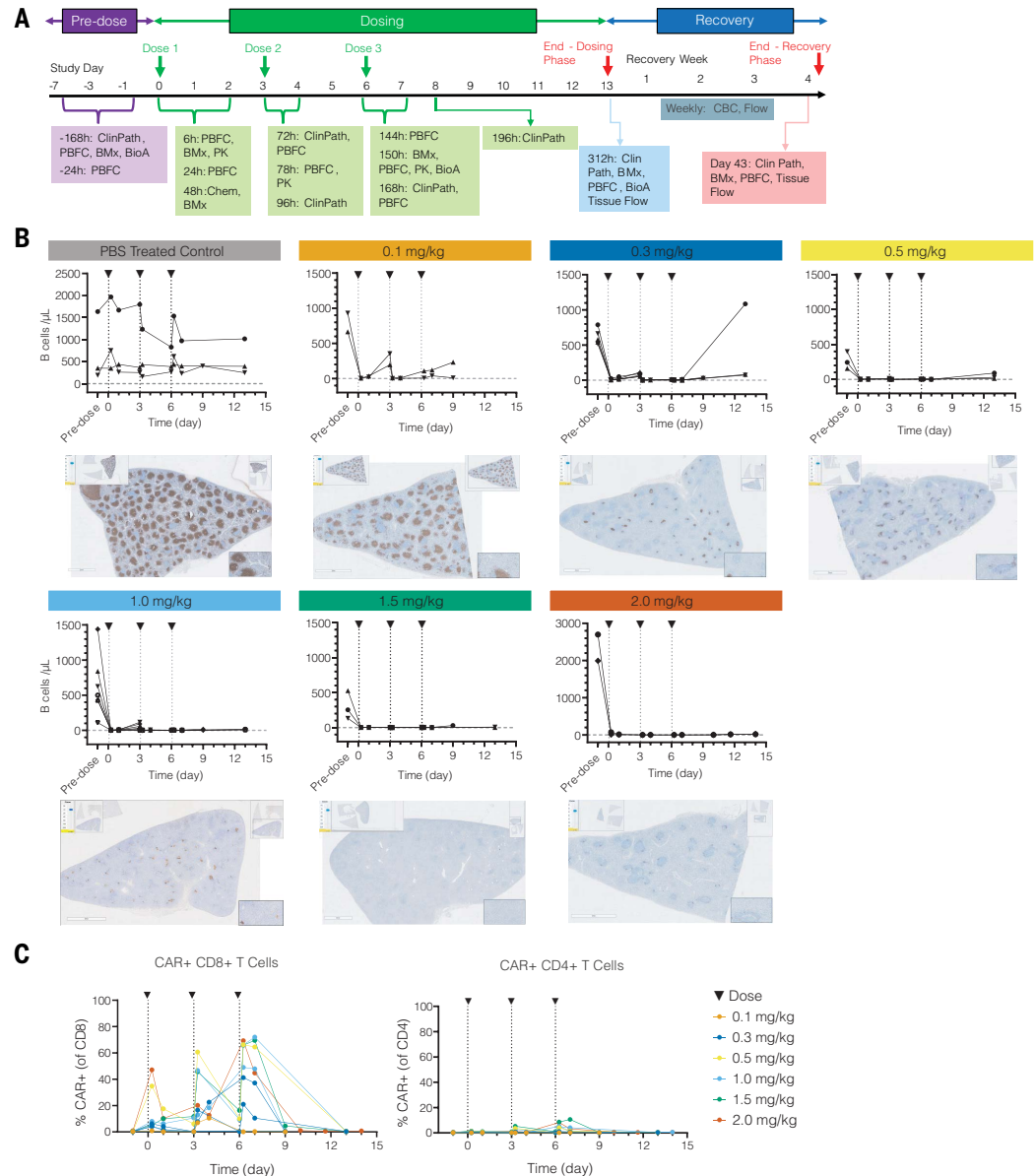


Fig. 3. tLNPs encapsulating B cell-targeted CAR induce rapid B cell depletion in autoimmune patient samples and humanized mice. (A) Expression of anti-CD19 CAR 24 hours after in vitro transfection with CD8-L829-tLNP-CD19 of nonactivated human T cells derived from autoimmune disease patients and healthy donors. (B) B cell depletion 72 hours after in vitro transfection with CD8-L829-tLNP-CD19 of nonactivated PBMCs derived from autoimmune disease patients and healthy donors. Killing is normalized to nontransfected controls. Differences between patients and healthy donors are not significant according to one-way ANOVA with post hoc multiple comparisons. Not all samples in (A) and (B) had sufficient material for testing in both assays. Samples from patients on B cell-depleting therapies were not included in this analysis because of <100 baseline B cells in the nontransfected control. Each dot represents a distinct donor, except for two dermatomyositis patients and one healthy donor who gave two to three samples at distinct time points. (C) Percent B cells of human CD45+ cells in the spleens of NSG-PBMC mice 24 hours after treatment with indicated doses of tLNP. n = 8 (mCherry) or 10 (anti-CD19 CAR) mice per group. (D) Time course showing the percentage of B cells among human CD45+ cells in the spleens of NSG-PBMC mice at 1, 3, 6, and 24 hours after treatment with 30 µg of the specified tLNPs. n = 5 (mCherry) or n = 10 (CAR) mice per group. (E) CAR expression on CD8+ T cells in the spleens of NSG-PBMC mice at 1, 3, 6, and 24 hours after administration of 30 µg of the indicated tLNPs. n = 5 (mCherry) or 10 (CAR) mice per group. (F) Percent of circulating B cells of human CD45+ cells in NCG-CD34+ humanized mice after three doses every 3 days of indicated tLNP. Statistical analysis by one-way (C) or two-way [(D) and (F)] ANOVA with post hoc multiple comparisons. (***P ≤ 0.001, ****P ≤ 0.0001; ns = not significant, P > 0.05). (G) Bioluminescence imaging of Nalm6 tumors in NCG mice engrafted with human PBMCs, taken at the indicated time point (lower panels) in mice treated with indicated tLNP. CD8-L829-tLNP-mCherry mice received 30 µg. Mice were randomized into groups on Day -1. n = 5 mice per group. Data are mean ± standard deviation.

Fig. 4. Treatment with tLNPs encapsulating B cell-targeted CAR mRNA induces deep B cell depletion in cynomolgus monkeys. (A)

Representative study schematic for three separate studies in which cynomolgus monkeys were given three doses of CD8-L829-tLNP-CD20 every 3 days. BioA, ADA and PK assays; BMx, biomarkers; ClinPath, clinical pathology consisting of complete blood count, serum chemistry, and coagulation testing; h, hour; PBFC, peripheral blood flow cytometry. **(B)** (Top) B cells/ μ l (CD19⁺ and/or CD20⁺) in blood after dosing cynomolgus monkeys with indicated amounts of CD8-L829-tLNP-CD20. Doses are indicated by arrows. Data combined from three studies. (Bottom) Representative spleen sections stained for CD20 through immunohistochemistry are shown for each dose group. Spleen samples were taken from animals 8 days (2.0 mg/kg), 7 days (PBS, 0.5, and 1.5 mg/kg), or 3 days (0.1, 0.3, and 1.0 mg/kg) after dose 3. **(C)** Averaged surface CAR expression on CD8⁺ T cells (left) and CD4⁺ T cells (right) for each dose group within each study, with a total of three studies. Separate lines of the same color represent the same dose groups from different studies, to account for varying time points and CD20 CAR detection reagent between studies.



mouse model. Mice treated with 30 μ g of CD8-L829-tLNP-CD19, administered every 3 days for three doses, exhibited rapid and sustained B cell depletion for up to 14 days after the initial dose compared with controls (Fig. 3F).

To test whether the tumor cell killing observed *in vitro* would translate to an *in vivo* setting, we utilized a humanized leukemia xenograft mouse model routinely used with *ex vivo* CAR T (25). Unlike *ex vivo* models that involve adoptive transfer of virally transduced CAR T cells, this model entailed engraftment of Nalm6 tumor cells alongside human PBMCs, allowing for *in vivo* T cell engineering. After PBMC engraftment and a 7-day tumor growth period, mice were imaged and randomized into groups based on tumor size and PBMC engraftment. Mice were then injected with 10 or 30 μ g of CD8-L829-tLNP-CD19 or 30 μ g of CD8-L829-tLNP-mCherry control, administered twice weekly for a total of five doses. The 10- μ g dose of CD8-L829-tLNP-CD19 resulted in considerable tumor control compared with the control group (Fig. 3G and fig. S5F). The 30- μ g dose led to near-complete tumor clearance in four of five animals by 2 days after the first dose and in all animals by 3 days after the second dose (Fig. 3G and fig. S5G).

These findings suggest that CD8-L829-tLNP-CD19 effectively generates functional CAR T cells capable of depleting B cells and eradicating tumors *in vivo*, with potential applicability in autoimmune disease treatment.

Deep B cell depletion and evidence of immune reset in cynomolgus monkeys

To evaluate the efficacy and safety of *in vivo* anti-B cell CAR T therapy in a translationally relevant model, we conducted studies in cynomolgus monkeys. The anti-CD8 antibody used to target human T cells is cross-reactive to cynomolgus CD8; however, the anti-CD19 binder of the CAR is not. To target cynomolgus monkey B cells, we utilized an anti-CD20 CAR that had been shown previously to deplete B cells in monkeys with an *ex vivo* lentiviral vector engineering approach (26). The improved anti-CD20 CAR mRNA, with sequence modifications as described, was encapsulated in L829-LNPs conjugated to the CD8 targeting antibody. *In vitro* assays confirmed that CD8-L829-tLNP-CD20 effectively engineered cynomolgus monkey T cells to target and eliminate cell lines expressing human or cynomolgus CD20 (fig. S6A).

Across three studies, 22 cynomolgus monkeys received intravenous doses of CD8-L829-tLNP-CD20 ranging from 0.1 to 2.0 mg/kg every 72 hours for a total of three doses (Fig. 4A and table S2). Animals were not pretreated with corticosteroids or antihistamines. Comprehensive clinical pathology and biomarker analyses were performed at all dose levels (figs. S6, B to D, and S7 to S10). The treatment was generally well tolerated; however, one monkey in the 1.5 mg/kg group was found lying prone, hypoaemic, and hypothermic 72 hours after the third dose and was humanely euthanized. Clinical and biomarker assessments at sacrifice were consistent with immune effector cell-associated hemophagocytic lymphohistiocytosis-like syndrome (figs. S8 and S10B), a recognized adverse effect of CAR T cell therapies (27). More common findings in the other animals included mild, transient elevations in liver enzymes, and cytokines such as interleukin-6 (IL-6), monocyte chemoattractant protein 1 (MCP-1), and interferon- γ (IFN γ), which are all consistent with on-target pharmacology expected with CAR T cell treatment (28). Transient increases in body temperature and C-reactive protein levels were also observed, which are consistent with typical responses to nanomedicine administrations. No central nervous system symptoms or seizures were observed.

Peripheral blood B cell counts declined sharply within 6 hours of the first dose and approached undetectable levels by 24 hours (Fig. 4B). Although sample size was limited at each dose level, CAR expression appeared dose-dependent, with up to 85% of CD8⁺ T cells and up to 95% of CD8⁺ NK cells expressing the CAR after the third dose, whereas minimal expression was observed on CD4⁺ T cells (Fig. 4C and fig. S11, A and B). A marked increase in the number of CD8⁺ T cells in the peripheral blood was also observed after the second dose (fig. S11C). Immunohistochemistry confirmed substantial B cell depletion in the spleen and lymph nodes in CD8-L829-tLNP-CD20-treated animals compared with controls (Fig. 4B and fig. S11D). In animals dosed with 1

to 1.5 mg/kg and monitored for B cell recovery, reemergence of B cells in peripheral blood began around day 21, returning to near baseline values by day 35 (fig. S12). Notably, memory B cells were largely eradicated and the posttreatment B cells that returned in the blood and tissues had a predominantly naïve phenotype (Fig. 5 and fig. S12), which is suggestive of immune reset, similar to what has been reported in autoimmune patients treated with ex vivo anti-CD19 CAR T cells (29).

To better characterize the therapeutic window, we explored a more compact dosing regimen in 15 additional cynomolgus monkeys (table S2), comparing only two doses spaced 72 hours apart with the three-dose schedule, and found that the two-dose schedule also achieved deep peripheral blood and tissue B cell depletion as effectively as a three-dose regimen, with returning B cells again predominantly naïve (fig. S13). The two-dose regimen also demonstrated a favorable safety and tolerability profile and avoidance of increases in IL-6, MCP-1, and IP-10 observed after a third dose (fig. S14). Furthermore, because patients receiving intravenous LNP products are routinely premedicated with low-dose corticosteroids and antihistamines (30, 31), in a separate study of four cynomolgus monkeys (table S2), we confirmed that premedicating before tLNP dosing did not interfere with in vivo CAR engineering rates or B cell depletion but did have an additional positive impact on the safety-related markers, as demonstrated by multifold reduction in C-reactive protein after tLNP infusion and decreased levels of cytokines, including IL-6, which is a key driver of CRS (fig. S15). Although sample sizes are small, these data provide rationale for compact dosing and premedication in future clinical studies.

Discussion

In this study, we introduced a novel CD8-L829-tLNP-CD19 formulation that preferentially engineers T cells in vivo to deplete B cells in humanized mice and cynomolgus monkeys. This depletion leads to repopulation with naïve B cells, which is suggestive of an immune reset. Clinical reports of ex vivo CAR T cell therapy in autoimmune patients have shown that although B cells return after ablation, symptoms often do not reappear (6, 8, 9). Returning B cells were shown to be predominantly naïve, suggesting that transient ablation of pathogenic B cells was sufficient to “reset” the immune system, providing a durable benefit (29). A key factor in this “reset” may be the depth of B cell depletion. B cell-depleting antibodies have shown incomplete depletion of B cells in tissues, which is thought to be why these therapies have not been as effective as CAR T cells in treating autoimmune patients (32–34).

However, CAR T approaches that use viral integrating vectors pose considerable challenges. First, long-term CAR expression from integrating vectors can lead to prolonged B cell aplasia, hypogammaglobulinemia, and cytopenia, increasing the risk of serious infections (35). Second, recent reports of T cell lymphomas in patients treated with CAR T cell therapy have prompted regulatory agencies, such as the FDA, to mandate lifetime monitoring for secondary malignancies for patients treated with integrating vectors (36–39). These concerns raise questions about the

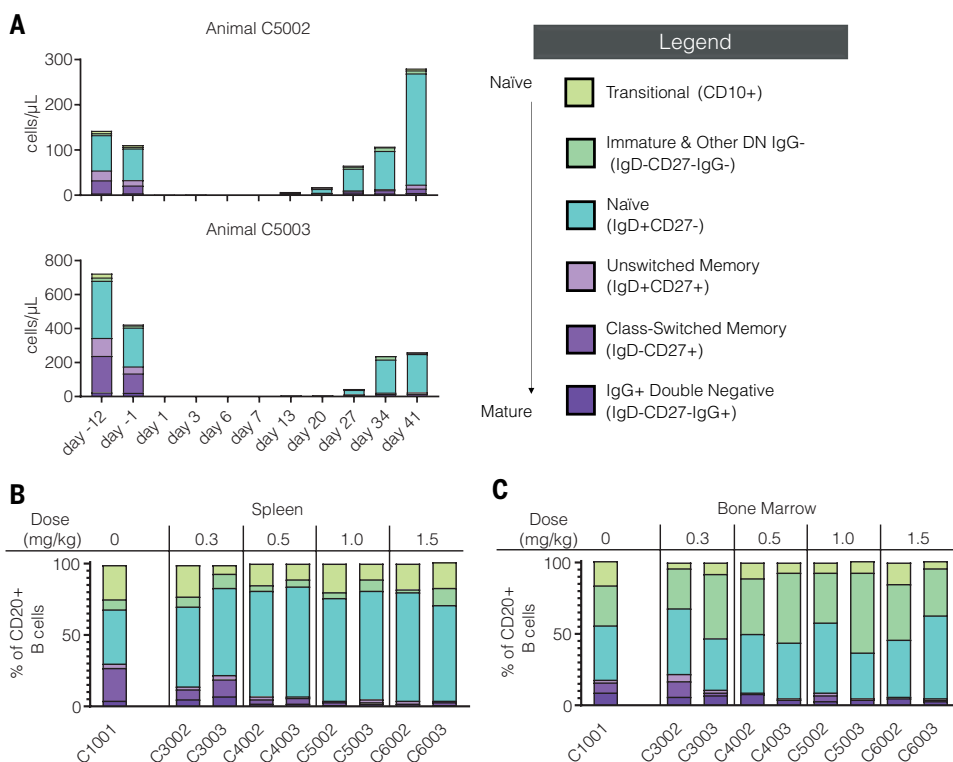


Fig. 5. Predominance of naïve B cells upon B cell lineage recovery after tLNP treatment-induced global B cell depletion. (A) Enumeration of B cell subsets (cells/ μ l) in blood over time in two cynomolgus monkeys dosed with 1.0 mg/kg CD8-L829-tLNP-CD20. DN, double negative; IgG, immunoglobulin G; IgD, immunoglobulin D. (B) Proportion of B cell subsets as percent of CD20⁺ cells in spleen and (C) bone marrow 5 weeks after last dose. Data shown are from one of three studies with $n = 2$ animals per group.

suitability of such therapies for autoimmune disease patients, especially in earlier treatment stages.

Our nonviral, scalable approach using tLNPs with transient mRNA payloads addresses these issues by potentially reducing long-term risks associated with integrating vectors. Although we identified two- and three-infusion regimens leading to the desired pharmacological effect and maintaining a favorable safety profile preclinically, key questions remain regarding the translatability of this approach to the clinic, including dose levels and regimens required to achieve immune reset in humans and the relationship between the B cell phenotype and function of repopulating cells and the durability of clinical response. In certain oncological indications, a more extensive treatment regimen consisting of repeat dosing over an extended period may be required to achieve a durable clinical response. These extended dosing regimens have not yet been explored and would need to be evaluated for the development of immunogenicity or antidrug antibodies against the tLNP, which could potentially limit the efficacy of repeat dosing over time. Additionally, in B cell-mediated autoimmune disease, determining whether this strategy should be reserved for refractory patients or used earlier in treatment is crucial. Overall, this *in vivo* approach offers the promise of potentially safer and more accessible CAR T therapies for B cell-mediated pathologies in oncology and autoimmune disease (27).

REFERENCES AND NOTES

1. V. Wang, M. Gauthier, V. Decot, L. Reppel, D. Bensoussan, *Cancers* **15**, 1003 (2023).
2. K. M. Cappell, J. N. Kochenderfer, *Nat. Rev. Clin. Oncol.* **20**, 359–371 (2023).
3. J. J. Melenhorst *et al.*, *Nature* **602**, 503–509 (2022).
4. A. Gajra *et al.*, *Pharmaceut. Med.* **36**, 163–171 (2022).
5. G. Schett, A. Mackensen, D. Mouggiakakos, *Lancet* **402**, 2034–2044 (2023).
6. C. Bergmann *et al.*, *Ann. Rheum. Dis.* **82**, 1117–1120 (2023).
7. D. Mouggiakakos *et al.*, *N. Engl. J. Med.* **385**, 567–569 (2021).
8. A. Mackensen *et al.*, *Nat. Med.* **28**, 2124–2132 (2022).
9. A.-C. Pecher *et al.*, *JAMA* **329**, 2154–2162 (2023).
10. A. Haghikia *et al.*, *Lancet Neurol.* **22**, 1104–1105 (2023).
11. N. Conrad *et al.*, *Lancet* **401**, 1878–1890 (2023).
12. M. H. Roberts, E. Erdei, *Autoimmun. Rev.* **19**, 102423 (2020).
13. F. W. Miller, *Curr. Opin. Immunol.* **80**, 102266 (2023).
14. J. G. Rurik *et al.*, *Science* **375**, 91–96 (2022).
15. L. Zhang *et al.*, *NPJ Vaccines* **8**, 156 (2023).
16. A. Kheirolomoom *et al.*, *Biomaterials* **281**, 121339 (2022).
17. M. M. Billingsley *et al.*, *Small* **20**, 2304378 (2024).
18. N. N. Parayath, S. B. Stephan, A. L. Koehne, P. S. Nelson, M. T. Stephan, *Nat. Commun.* **11**, 6080 (2020).
19. M. Sedic *et al.*, *Vet. Pathol.* **55**, 341–354 (2018).
20. Z. Good *et al.*, *Nat. Med.* **28**, 1860–1871 (2022).
21. V. R. Moulton, G. C. Tsokos, *J. Clin. Invest.* **125**, 2220–2227 (2015).
22. M. Boulch *et al.*, *Cell Rep. Med.* **4**, 101161 (2023).
23. J. N. Brudno *et al.*, *Nat. Med.* **26**, 270–280 (2020).
24. L. Alabanza *et al.*, *Mol. Ther.* **25**, 2452–2465 (2017).
25. D. M. Barrett *et al.*, *Hum. Gene Ther.* **22**, 1575–1586 (2011).
26. A. Taraseviciute *et al.*, *Cancer Discov.* **8**, 750–763 (2018).
27. M. R. Hines *et al.*, *Transplant. Cell. Ther.* **29**, 438.e1–438.e16 (2023).
28. E. C. Morris, S. S. Neelapu, T. Giavridis, M. Sadelain, *Nat. Rev. Immunol.* **22**, 85–96 (2022).
29. F. Müller *et al.*, *N. Engl. J. Med.* **390**, 687–700 (2024).
30. M. T. Abrams *et al.*, *Mol. Ther.* **18**, 171–180 (2010).
31. I. Urits *et al.*, *Neurol. Ther.* **9**, 301–315 (2020).
32. T. H. Ramwadhoebe *et al.*, *Rheumatology* **58**, 1075–1085 (2019).
33. M. Nakou *et al.*, *Arthritis Res. Ther.* **11**, R131 (2009).
34. C. Tur *et al.*, *Ann. Rheum. Dis.* **84**, 106–114 (2024).
35. A. G. Stewart, A. S. Henden, *Ther. Adv. Infect. Dis.* **8**, 20499361211036773 (2021).
36. M. Suran, *JAMA* **331**, 818–820 (2024).
37. G. Ghilardi *et al.*, *Nat. Med.* **30**, 984–989 (2024).
38. C. J. Nicolai *et al.*, *Blood* **144**, 977–987 (2024).
39. N. Verdun, P. Marks, *N. Engl. J. Med.* **390**, 584–586 (2024).

ACKNOWLEDGMENTS

We thank C. Bentley for discussion and comment on the manuscript, M. Khoshnejad for RNA sequence support, Invivico for generating the luciferase biodistribution data, and Aliri Bioanalysis for generating the tissue lipid LC-MS data. **Funding:** This research was supported by Capstan Therapeutics (“Capstan”), including the work done by J.S. and C.H.J. under a sponsored research agreement with the University of Pennsylvania. Capstan participated in the design and conduct of the study, analysis and interpretation of data, the preparation and review of the manuscript, and the decision to submit the manuscript for publication. This study was funded in part by the Intramural Research Program of the National Institute of Arthritis and Musculoskeletal and Skin Diseases, NIH. **Author contributions:** Investigation: T.L.H., Y.Z., R.R., A.W., F.S., D.P.N., B.R., J.V., D.G., D.J., M.B., J.N., S.Z., C.F., J.C., C.H., Y.K., E.M.P., G.M.; Methodology: T.L.H., Y.B., Y.Z., D.M., R.R., A.W., J.J.L., F.S., D.S.H.C., D.P.N., Q.C.Y., M.N., S.R., J.B.V., S.A.S., A.M.F., G.B.A., P.P.K., A.I.B., C.H.J., H.A.; Project administration: T.L.H., Y.B., Y.Z., D.M., R.R., A.W., J.J.L., D.S.H.C., Q.-C.Y., M.N., S.R., J.B.V., M.B., C.F., G.M., S.A.S., A.M.F., G.B.A., P.P.K.; Resources: A.L.M.; Supervision: J.S., S.P.T., S.A.S., A.M.F., G.B.A., L.S., R.F.-F., M.R., P.P.K., A.I.B., C.H.J., H.A.; Visualization: T.L.H., Y.Z., R.R., A.W., F.S., B.R., D.G., J.N.; Writing – original draft: T.L.H., H.A.; Writing – review & editing: T.L.H., Y.B., Y.Z., D.M., R.R., A.W., J.J.L., F.S., D.S.H.C., D.P.N., Q.-C.Y., B.R., M.N., J.V., S.R., D.G., J.B.V., D.J., M.B., J.N., S.Z., C.F., J.C., C.H., Y.K., E.M.P., G.M., A.L.M., J.S., S.P.T., S.A.S., A.M.F., G.B.A., L.S., R.F.-F., M.R., P.P.K., A.I.B., C.H.J., H.A. **Competing interests:** T.L.H., Y.B., Y.Z., D.M., R.R., A.W., J.J.L., F.S., D.S.H.C., D.P.N., Q.-C.Y., B.R., M.N., J.V., S.R., D.G., J.B.V., D.J., M.B., J.N., S.Z., C.F., J.C., C.H., Y.K., E.M.P., G.M., S.P.T., S.A.S., A.M.F., G.B.A., L.S., R.F.-F., M.R., P.P.K., A.I.B., and H.A. are employees of Capstan Therapeutics. S.P.T. is a consultant for BIOIO Tech. A.L.M. is an advisory board member for Cure JM. C.H.J. holds patents related to CAR T cells and is a scientific cofounder of Capstan Therapeutics, Bluewhale Bio, and Dispatch Bio, and is a member of the scientific advisory boards of AC Immune, BluesphereBio, Cabaletta, Cartography, Cellares, Celldex, Decheng, Verismo, and WIRB-Copernicus. P.P.K. and S.P.T. are listed as inventors on patent application WO 2023/196444 submitted by Capstan Therapeutics, which covers novel ionizable cationic lipids. P.P.K., S.P.T., and Y.B. are listed as inventors on patent application WO 2024/249954 submitted by Capstan Therapeutics, which covers lipid nanoparticle formulations and compositions. D.M., Y.Z., D.P.N., Q.-C.Y., P.P.K., S.A.S., A.I.B., and H.A. are listed as inventors on patent application WO 2025/096878 submitted by Capstan Therapeutics, which covers improved RNA sequences. **Data and materials availability:** All data are available in the main text or the supplementary materials. **License information:** Copyright © 2025 the authors, some rights reserved; exclusive licensee American Association for the Advancement of Science. No claim to original US government works. <https://www.science.org/about/science-licenses-journal-article-reuse>

SUPPLEMENTARY MATERIALS

science.org/doi/10.1126/science.ads8473

Materials and Methods; Figs. S1 to S15; Tables S1 and S2; References (40, 41); Data S1 and S2; MDAR Reproducibility Checklist

Submitted 31 August 2024; resubmitted 3 February 2025; accepted 1 May 2025

10.1126/science.ads8473